Skewness and critical current behavior in a graphene Josephson junction

Diego A. Manjarrés,[1,2,*] Shirley Gómez Páez,[1,2] and William J. Herrera[1]
[1]*Departamento de Física, Universidad Nacional de Colombia, 111321, Bogotá, Colombia*
[2]*Departamento de Física, Universidad El Bosque, 110121, Bogotá, Colombia*

(Received 5 October 2018; accepted 9 January 2020; published 4 February 2020)

In this work, the DC Josephson effect is investigated for a superconductor-graphene-superconductor junction in both short- and long-junction regimes. The electric transport properties are calculated while taking into account the contribution of the discrete and continuous energy spectrum. In our approach, the phase dependence of the critical current is calculated at arbitrary temperature and doping level, which generalizes previous results. We show that critical current I_c and skewness S exhibit critical points as a function of graphene doping E_F, which can be explained by Klein resonances in graphene. We give a general characterization of S vs I_c curves while fixing temperature or doping level. When the temperature dependence of I_c is analyzed, we find differences with respect to conventional Josephson junctions, given that there is a relevant doping effect. In the long-junction regime with E_F far away from the Dirac point, the I_c vs T curve may exhibit an exponential decay law, which has been measured recently. We report the temperature dependence of S in the whole range of temperature, and our approach allows us to account for skewness suppression in the vicinity of the Dirac point, which is in agreement with recent experiments. We mention some effects which can be attained in Josephson junctions with well-defined edges and for transparency values below unity of the graphene-superconductor interfaces.

DOI: 10.1103/PhysRevB.101.064503

I. INTRODUCTION

The Josephson effect in superconductor-graphene-superconductor (SGS) junctions has been investigated by several authors [1–5], who demonstrated that graphene as a weak link can support a dissipationless supercurrent. For junctions in the short limit, current transport is mediated mainly by discrete Andreev levels through successive Andreev reflections [6]. In the opposite long-junction regime, the contribution of the continuum must be included. One of the main features of the Josephson junction is the current-phase relation (CPR) [7], which gives information about the coupling between superconductors and superconducting properties and can be used as a merit figure for Josephson devices. The CPR can be forward skewed, and its deviation of sinusoidal behavior is measured by a dimensionless parameter named skewness S. A recent review [8] summarized the advances in understanding CPR in graphene Josephson junctions.

The fact that for potential barriers in graphene, we can have a perfect transmission or Klein tunneling [9] for incident electrons with energies below barrier height suggests that an analysis of CPR in SGS junctions is necessary. It is well known how transmission resonances appear in nonsuperconducting graphene systems with barriers [10,11] and quantum wells [12]. The role of Klein and non-Klein processes and their respective contribution to transmission has been analyzed [13] in double-barrier systems where electrostatic-based barriers take into account Klein processes. There are different transmission processes that involve propagating and evanescent states, from discrete and continuous energy spectra, which can mediate supercurrent transport across the junction.

The Josephson effect has been measured in the ballistic regime [3,5,14–17]; there are Fabry-Pérot interference effects in graphene, which lead to critical current oscillations as a function of gate voltage. Other works considered long junctions [18–20], for which the temperature dependence of I_c and some current phase relationships were analyzed but only some doping values were considered. Recent progress includes the experimental measurement of skewness [14,21], showing how S oscillates as a function of E_F and the full temperature dependence of S. Several authors discussed the temperature dependence of the critical current [18–20]. Recently, some experiments [15] with encapsulated graphene gave guidelines to clarify the discussion of ballistic junctions; within a certain temperature range, an exponential decay of the critical current for long junctions [15] has been measured, similar to the result for conventional Josephson junctions.

In Josephson junctions the competition between Klein and non-Klein processes has not been studied; this work shows how nanoribbon bound states can influence the Josephson supercurrent, and an explanation of concavity changes in the critical current as a function of doping is given and related to Klein resonances. Our model accounts for skewness suppression near the Dirac point where other models fail [14]. Our approach allows us to consider both short- and long-junction regimes at arbitrary temperature and doping, thereby giving a complete description of CPR in graphene Josephson junctions. Our analysis clarifies I_c vs T dependence and the parameter values for which behavior changes; in the long-junction regime I_c temperature dependence obeys an exponential decay law in the low range of temperature, which resembles the temperature behavior of

*damanjarrnsg@unal.edu.co

SNS (S: superconductor, N: normal metal) junctions. For low transparency values of GS interfaces, I_c exhibits oscillations as a function of doping, and junctions with zigzag edges exhibit a different behavior at low doping values.

We expect that the Josephson effect in nanostructures with well-defined edges between graphene-superconductor interfaces will become relevant in nanoelectronics. Our approach allows us to consider zigzag or armchair edges at graphene-superconductor interfaces. Most research on the SGS Josephson effect does not make a distinction between armchair and zigzag, which can give some different features. Nanoribbons with armchair and zigzag edges were synthesized a few years ago [22,23], and recently, there have been advances in large-scale production of zigzag nanoribbons [24,25], which are promising for nanoelectronics.

In Sec. II we introduce the theoretical approach used in this work; the electric transport properties at finite temperature are calculated through Green's function formalism, which generalizes and extends previous results [18–20]. An integral expression for the current can be obtained for the zigzag case, where the phase dependence is given explicitly. For the armchair case the Dyson equation is solved numerically. We consider in some cases nonideal graphene-superconductor interfaces, which can be modeled through the hopping parameter between interfaces. Section III A shows that I_c and S as a function of E_F exhibit critical points, which are correlated. We employ a model based on Klein tunneling to explain I_c behavior and the local maxima and minima that arise in skewness. For nonideal interfaces, we show that the edge effect is noticeable, where curves are out of phase, and for low doping values the critical current exhibits amplitude differences. In Secs. III B and III C the temperature dependence of the critical current and skewness is analyzed in both short- and long-junction regimes, where different features arise when graphene doping is varied.

II. THEORETICAL MODEL

Although graphene is not a superconductor, we can model the superconducting regions with the honeycomb lattice structure. Between superconductors, there is phase difference φ, and the weak link length is L, which is much smaller than its width (see Fig. 1). We consider translational invariance along the y axis. The length L is determined by the location of the superconducting leads, which are deposited on the graphene film; the ellipsis indicates that we are not restricted to any particular junction length. For simplicity, we consider a geometry in which graphene-superconductor interfaces have armchair or zigzag edges. The current transport is transverse to the edges. Figure 1 illustrates an armchair edge, but both edge types are considered in our model.

The coupling between normal and superconducting graphene regions is modeled through the Hamiltonian approach, which takes into account the different dispersion processes. The normalized hopping parameters between interfaces $P_L = t_L/\hbar v_F$, $P_R = t_R/\hbar v_F$ are related to interface transparency through

$$T_{L(R)} = \frac{4P_{L(R)}}{(1+P_{L(R)})^2}; \tag{1}$$

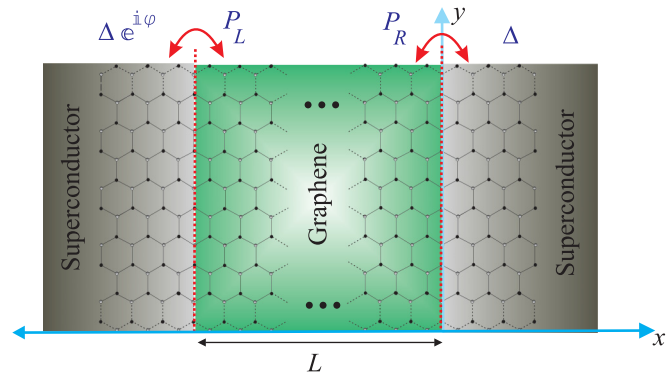

FIG. 1. The Josephson SGS junction, with edges transverse to the current transport direction along the x axis. The diagram illustrates that along the y axis, graphene-superconductor interfaces have armchair edges, but zigzag edges are also considered in this work. The normalized hopping values for the left and right interfaces are P_L and P_R, respectively. There is a phase difference of φ between superconductors, and the junction length is L. The dashed lines represent that structure extends along the y axis and that in general the junction width W is larger than L. The three dots mean that we do not focus on ultrashort Josephson junctions.

by varying the parameter $P_{L(R)}$ in our model we consider imperfect interfaces. T must be distinguished from the effective transmission throughout the junction, which is proportional to the Josephson supercurrent. The Fermi vector mismatch between normal and superconducting regions can be modeled as a potential barrier, $V_0 = E_{FS} - E_F$.

The current is calculated from perturbed Green's functions for the SGS junction. We start from nonperturbed Green's functions for graphene regions; these Green's functions are obtained from asymptotic solutions of the Bogoliubov–de Gennes–Dirac Hamiltonian [26]. The equilibrium-perturbed Green's function for the SGS junction is obtained by solving the Dyson equation. The current between the two regions, left L and right R, is given by

$$I = \frac{e}{h}\int_{-\infty}^{\infty}\int_{-k_c}^{k_c} \mathrm{Tr}[A]\,dk_y dE, \tag{2}$$

with

$$A = \check{\sigma}_z[\tilde{\Sigma}_{LR}\tilde{G}^{+-}_{RL}(E,k_y) - \tilde{\Sigma}_{RL}\tilde{G}^{+-}_{LR}(E,k_y)], \tag{3}$$

where $\check{\sigma}_z = \hat{\sigma}_z \otimes I$, with $\hat{\sigma}_z$ being the Pauli matrix and $\otimes$ being the tensor product which arises due to Nambu and sublattice space. $\tilde{\Sigma}_{LR}$, $\tilde{\Sigma}_{RL}$ are self-energies which connect the left and right regions, and their structure depends on the interface, zigzag or armchair edges. In equilibrium, the Keldysh Green's functions $\tilde{G}^{+-}_{RL}(E,k_y)$ and $\tilde{G}^{+-}_{LR}(E,k_y)$ are proportional to the Fermi-Dirac distribution function, which guarantees that for the DC Josephson effect only Green's perturbed equilibrium functions are necessary. Equation (2) takes into account the contributions of discrete Andreev levels and the continuous spectrum; propagating and evanescent states are included in the calculation with a cutoff value k_c. Therefore, this is a robust method to calculate the current through a junction; additionally, by solving the Dyson equation, we consider the

general case in which the order of perturbation series is taken up to infinity.

For an SGS Josephson junction with a zigzag edge, it is possible to obtain an integral expression for the current as

$$I(\varphi) = \frac{8e}{h} P_L^2 P_R^2 \sin\varphi \int_0^{\infty} \int_{-k_c}^{k_c} H(E, k_y, \varphi) dk_y dE, \quad (4)$$

where

$$H(E, k_y, \varphi) = \frac{\Delta^2}{\Omega^2}[2f(E) - 1]\mathrm{Im}\left[\frac{d_e d_h}{D_1 D_2(\varphi)}\right], \quad (5)$$

$$D_2(\varphi) = -1 - 2P_L^2 G(E, k_y)\cos\varphi + F(E, k_y), \quad (6)$$

$f(E)$ is the quasiparticle Fermi-Dirac distribution, Im denotes the imaginary part, and the quantities $d_e, d_h, D_1, G(E, k_y)$, and $F(E, k_y)$ are defined in Appendix. Equation (4) is a general expression for the current-phase dependence which complements previous works [2]; it is valid in both short- and long-junction regimes and for different values of doping and temperature. The result exhibits a nonsinusoidal dependence; the $\sin\varphi$ factor is accompanied by a nontrivial dependence on the phase difference given by Eq. (6).

In the tunnel limit the factor $D_2(\varphi)$ is φ independent, and therefore, sinusoidal behavior is recovered. We characterize CPR of the graphene Josephson junction through two parameters: the critical current $I_c = I(\varphi_{\max})$, which corresponds to the maximum value of the current, and skewness S, which gives information about the $\varphi_{\max}$ shift with respect to the $\pi/2$ value. Following the convention of other theoretical and experimental works, S is calculated via

$$S = \frac{2\varphi_{\max}}{\pi} - 1. \quad (7)$$

For a tunnel Josephson junction CPR has sinusoidal behavior ($S = 0$); by contrast, for systems with high-transmission states, CPR tends to have a sawtooth ($S = 1$) shape. Usually, graphene superconductor interfaces have high transmittance. Therefore, S values are expected to be higher for SGS systems in comparison with those obtained for SNS Josephson junctions. The presence of high-transmission states in the SGS junction results in a skewed forward CPR.

III. RESULTS AND DISCUSSION

A. Critical current and skewness behavior

Figure 2(a) plots I_c as a function of graphene doping for different transparency values of graphene-superconductor interfaces, considering both armchair and zigzag edges; the critical current values are normalized to $I_0 = e\Delta_0/\hbar$, with $\Delta_0 = \Delta(T = 0)$. For transparent interfaces, $T = T_L = T_R = 1$, we find that I_c increases monotonically, and the current curve exhibits inflection points, similar to previous results for short junctions in the ballistic regime [27]. There are two types of inflection points which give information about concavity change; in our analysis we name positive to negative concavity change type I and the opposite one type II. Figure 2(a) shows that type I inflection points are located at values whose difference is a number close to π.

An analysis of Klein tunneling in graphene systems with a potential barrier showed that transmission probability is equal

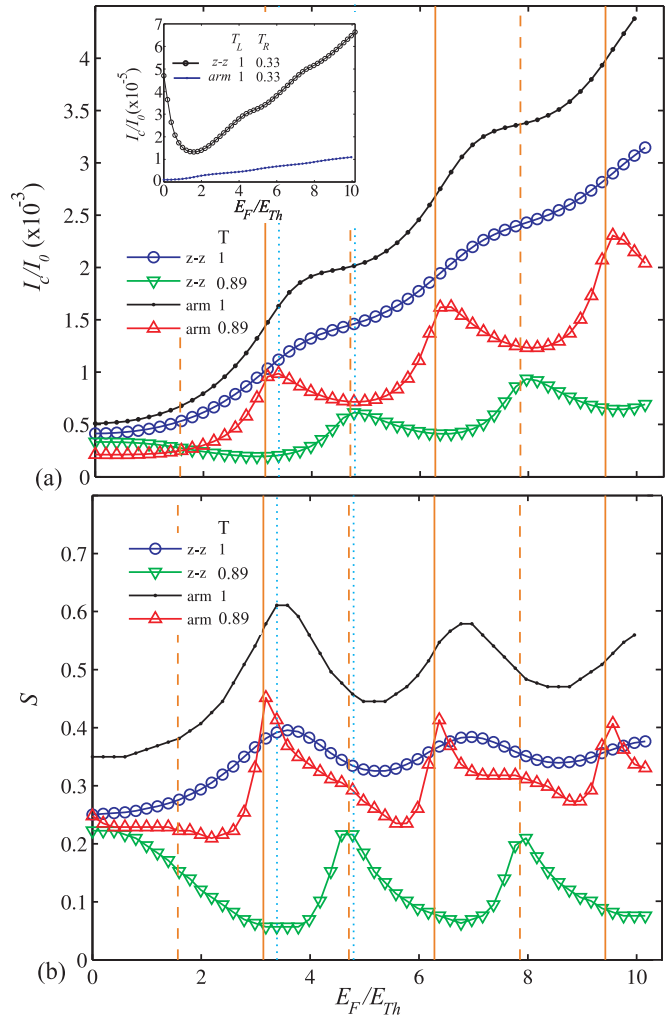

FIG. 2. (a) Critical current and (b) skewness as a function of graphene doping E_F for both armchair (arm) and zigzag (z-z) edges of graphene. The junction length is such that $L/\xi \approx 1.593$. The solid and dashed lines represent the values given by Eqs. (8) and (9). The dotted lines correspond to the location of the maxima and minima of I_c for the nonideal case. The inset in (a) illustrates the behavior when $T_L = 1$ and $T_R = 0.33$, where the zigzag case exhibits different behavior.

to unity for particular values of the incident wave number [11]. For normal incidence and zero excitation energy, the resonance condition reduces to

$$\frac{E_F}{E_{Th}} = n\pi, \quad n = 1, 2, \ldots, \quad (8)$$

with $E_{Th} = \hbar v_F/L$ being the Thouless energy. Values predicted by Eq. (8) are represented as solid lines in Fig. 2. The Josephson junction must inherit certain properties of graphene resonant structures; therefore, the critical current behavior can be explained by Klein resonances. The type I point is related to the Klein resonance condition (8); the derivative dI_c/dE_F has a maximum where for values of E_F/E_{Th} in the vicinity of the critical point, the transmission probability is equal to unity. Equation (4) takes an integral over excitation energy and wave number considering the different modes that satisfy the Klein resonance condition. The type II point is related to

the condition in which probability transmission is zero for $k_y = 0$; thus, the derivative dI_c/dE_F has a minimum. The monotonic increment of I_c is explained by the inclusion of more normal modes as E_F is increased; therefore, the resulting curve exhibits inflection points.

Figure 2(b) plots S as a function of E_F/E_{Th} for different transparency values at graphene-superconductor interfaces. The different curves exhibit oscillations as a function of graphene doping; we can explain local maxima for S through Klein resonances given by Eq. (8), where states with high transmission probability can produce a forward deviation of sinusoidal behavior and therefore a higher S value. For $T = 1$, we can observe from Fig. 2(b) that qualitatively, S behavior is the same for both edge types, and the period of oscillations is close to π; there is a shift in maxima and minima locations, and the differences are due to an average over energy and transversal wave number. Our model accounts for S suppression in the vicinity of the Dirac point, which was not explained by other models [14]; therefore, our results are in agreement with experimental results [14,21].

For nonideal interfaces $T = 0.89$, quasibound states of the nanoribbon play a role, and their associated quantization conditions are relevant [28]. In this situation, the critical current curve has a transition from inflection points to local maxima and minima, where the period is near π. The dotted lines in Fig. 2(a) correspond to the location of the first local maxima and minima of I_c, which are depicted to make a comparison with predictions of Klein resonances (solid lines). The armchair and zigzag curves are out of phase; the reason is that the armchair quantization condition of quasibound states is equivalent to Eq. (8), while for the zigzag case the following is obtained:

$$\frac{E_F}{E_{Th}} = \frac{n\pi}{2}, \quad n = 1, 3, 5, \ldots; \tag{9}$$

values predicted by Eq. (9) are represented as dashed lines in Fig. 2 and correspond to the location of local maxima of the critical current and skewness for the zigzag case. The predictions of Eqs. (8) and (9) give values close to the location of maxima and minima, as can be seen in Fig. 2. The critical current oscillations are a signature of ballistic transport in the Josephson junction; in this work we are able to explain the behavior exposed on the basis of Klein resonances and quantization conditions of bound states. The skewness also exhibits an oscillating behavior where the location of maxima and minima can be explained by Eqs. (8) and (9); for nonideal interfaces in comparison with the transparent case, the curves are narrower. The characteristics of graphene-superconductor interfaces are crucial, where for nonideal interfaces, the curves are out of phase for zigzag and armchair edges.

We can observe in Fig. 2 that critical points of the I_c and S curves are correlated, which is because of the contribution of high-transmission states. For ideal interfaces $T = 1$, the inflection points of the I_c curve are correlated with maxima and minima of the S curve (see Fig. 2), where concavity changes in I_c determine the type of critical point in S. For the nonideal case $T = 0.89$, local maxima of the I_c curve are a consequence of high-transmission states and therefore are associated with local maxima in the S curve.

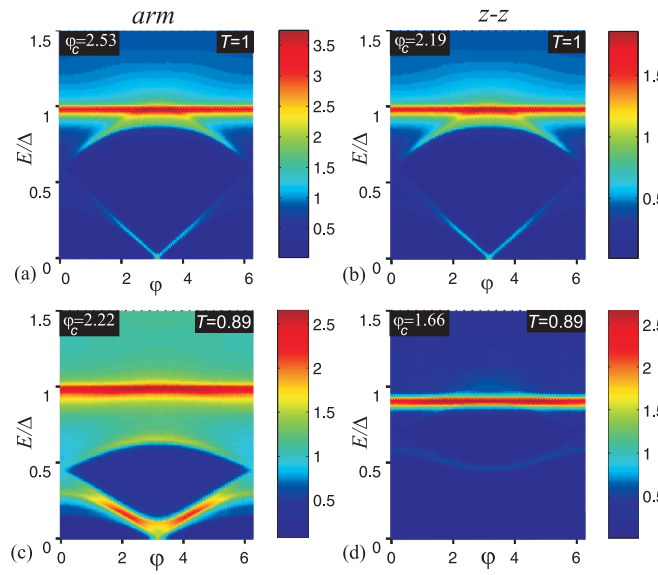

FIG. 3. The density of states as a function of energy and superconducting phase difference φ for both armchair and zigzag edges. The phase values indicated correspond to the critical phase values which maximize supercurrent. The junction length is such that $L/\xi \approx 1.593$. T is the transparency value at graphene superconductor interfaces. In (a)–(d) $E_F/\Delta_0 = 2.125$.

We can examine the local density of states integrated over the transversal wave number k_y as a function of energy and superconducting phase difference φ, which is shown in Fig. 3. The left and right columns correspond to the armchair and zigzag edges, respectively. Each density plot indicates the critical phase values which maximize supercurrent and transparency values for ideal ($T = 1$) and nonideal ($T = 0.89$) interfaces. The density plots give information about the phase dispersion of quasibound states, which allows performing an analysis of the current. The doping value considered is $E_F/\Delta = 2.125$, in which I_c exhibit the first local maxima and minima [dotted lines in Figs. 2(a) and 2(b)]. For $T = 1$ [Figs. 3(a) and 3(b)], we can observe that density plots exhibit qualitatively the same behavior, in contrast to $T = 0.89$ [Figs. 3(c) and 3(d)], in which the differences between zigzag and armchair cases are clear. The latter explains the change from the monotonic to oscillating behavior of I_c. The phase dispersion analysis of Fig. 3 can explain why Fig. 3(c) corresponds to local maxima in Fig. 2(a) while Fig. 3(d) is associated with local minima. The above can be seen from the following relation for the supercurrent [6,29] carried by quasibound states:

$$I_n(\varphi) = \frac{2e}{\hbar}\frac{\partial E_n}{\partial \varphi}. \tag{10}$$

Furthermore, we can see from Fig. 2(a) that behaviors for both types of edges are similar and the current amplitude is bigger for the armchair edge. However, for nonideal interfaces, the I_c behavior is different, where the current exhibits local maxima and minima and curves for armchair and zigzag edges are out of phase with each other. We consider contributions of both evanescent and propagating modes; the relative weight depends on the junction length L, doping level, and the

hopping parameter through interfaces. Low current values are obtained when doping is located at the Dirac point (zero doping) because in this case the transport is mediated mainly by evanescent states. For ideal interfaces, there are amplitude differences between short- and long-junction regimes, and behavior near the Dirac point is different, but in general, critical current curves have a universal behavior, where the locations of inflection points are the same.

Some authors [2,5,14] pointed out that there is a discrepancy between experimental and theoretical values of the critical current. In addition to this, we must mention that in Josephson junctions with well-defined edges, our results show that there are differences in amplitude between the armchair and zigzag cases, where values are greater for the armchair edge with transparent interfaces. When low values of transparency $T_R = 0.33$ are considered, the critical current is higher for the zigzag edge [see the inset in Fig. 2(a)], and it is achievable in the whole range of doping. Figure 2(a) shows that for low doping values $E_F/E_{Th} < 2$ and $T = 0.89$; I_c is higher for the zigzag case. It is worth mentioning that our results for the zigzag case in the short limit are in agreement with the value $S = 0.25$ predicted for a ballistic Josephson junction [27] with the doping level located at the Dirac point. For armchair interfaces, our calculations predict S values higher than previous results [19,20] in both short- and long-junction regimes.

B. Skewness vs critical current behavior

Figure 4(a) shows S vs I_c for short-, intermediate-, and long-junction regimes, with doping $E_F/\Delta = 10$. In comparison with previous work [19], our results extend the temperature range, and it is possible to obtain higher S values near zero temperature. For larger junctions the curve slope increases, which is expected due to coherence loss. Only for lower I_c values could the behavior be linear [19]. Therefore, experiments must be realized in the lower-temperature range, with the purpose being to observe the nonlinear behavior in which S has higher values. Additionally, our calculations indicate that for lower doping values the S vs I_c curve has higher slope values because of critical current decreases. The results are strongly affected by states in the continuum where S and I_c behavior with temperature changes. The continuous spectrum strongly influences the current-phase relation where transmission values for dispersion processes at graphene superconductor interfaces can be significantly different from those obtained for discrete Andreev levels.

In Fig. 4(b) each curve shows the behavior of S as a function of I_c when temperature is constant, and the doping value is varied for a short junction, $L/\xi \approx 0.1992$, with an armchair edge. The different curves exhibit a slightly skewed oscillating behavior, which can be explained by observing how for the ideal case $T = 1$, the S and I_c curves in Fig. 2 depend on the parameter E_F/E_{Th}. The oscillations seen in Fig. 4(b) are more pronounced when the temperature is decreased since in the proximity of zero temperature the biggest deviation of sinusoidal behavior is expected.

C. Temperature behavior

Figures 5(a) and 5(b) plot the critical current as a function of temperature for both armchair and zigzag edges in the

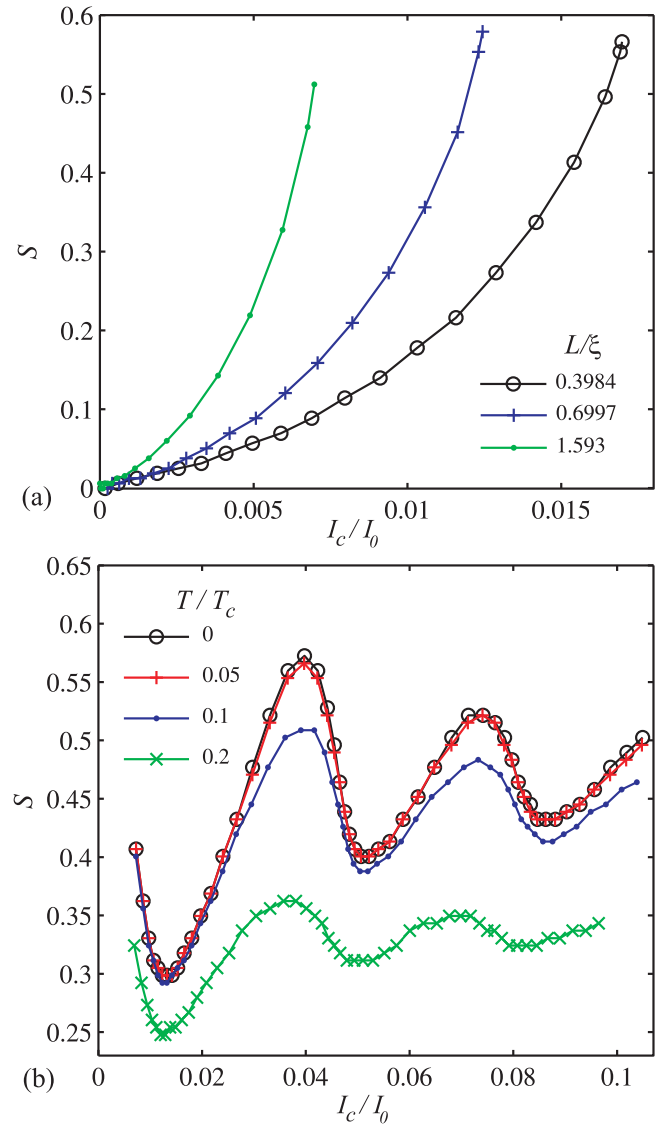

FIG. 4. Skewness as a function of critical current for an SGS junction. In (a) for each curve doping is constant, $E_F/\Delta_0 = 10$, and temperature changes; three different cases are depicted, $L/\xi \approx 0.3984, 0.6997, 1.593$. In (b) for each curve temperature is constant $T/T_c = 0, 0.05, 0.1, 0.2$, E_F changes, and $L/\xi \approx 0.1992$. The junction has an armchair edge.

short- and long-junction regimes, respectively. For the short junction $L < \xi$, with E_F located at the Dirac point, the behavior obtained qualitatively resembles results for SIS (S: superconductor, I: insulator) tunnel junctions and conventional superconductor-constriction-superconductor (ScS) junctions [7,30]. In this case the behavior is mainly influenced by evanescent states; therefore, the results of classical Josephson junctions with short normal regions are expected. In contrast, for $E_F/\Delta = 10$ [see the inset in Fig. 5(a)] the behavior exhibits a concavity change, which can be explained by modes that appear when doping is increased. For the long-junction regime $L > \xi$ [see Fig. 5(b)], a concavity change is also present, and the I_c temperature dependence does not exhibit a "plateau" at low temperatures; in this case the continuum is more relevant and influences CPR, where I_c decreases and S

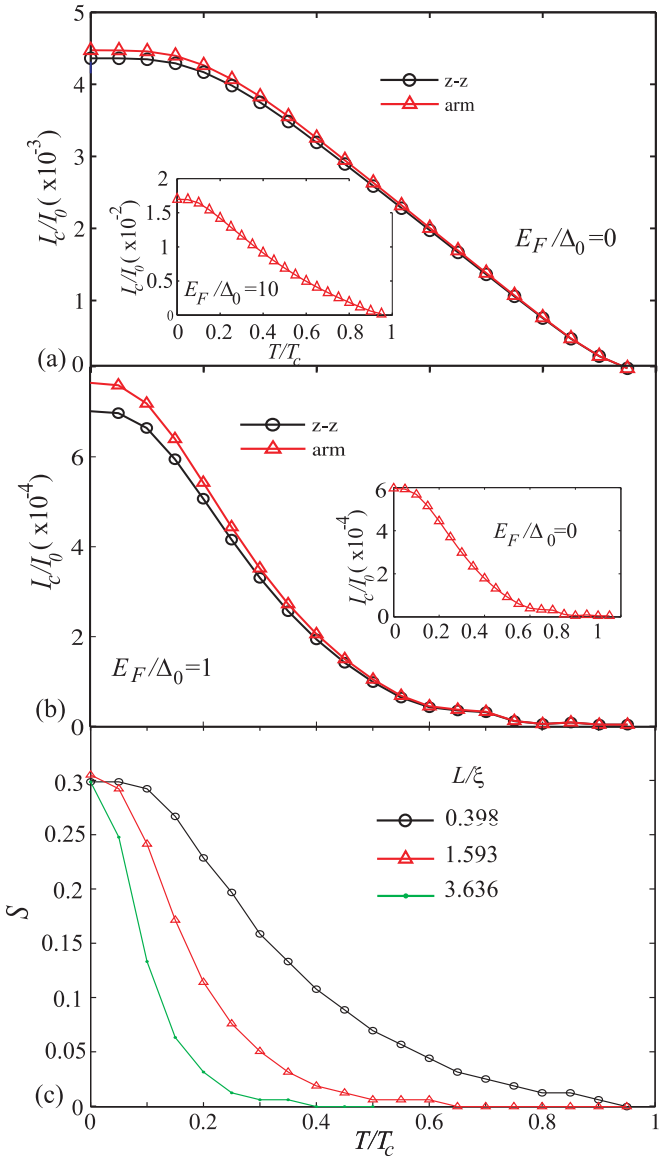

FIG. 5. Temperature dependence of critical current and skewness for an SGS Josephson junction with transparent interfaces $T = 1$. Both types of edges armchair (arm) and zigzag (z-z) are considered. In (a) $L/\xi \approx 0.398$, and $E_F/\Delta_0 = 0$; the inset illustrates the case $E_F/\Delta_0 = 10$. In (b) $L/\xi \approx 1.593$, and $E_F/\Delta_0 = 1$; the inset illustrates the case $E_F/\Delta_0 = 0$. In (c) the skewness behavior is plotted for the zigzag edge at the Dirac point for different junction lengths.

increases. The latter reflects the fact that sinusoidal behavior is suppressed as states with high transparency are included. Conversely, the evanescent states have an opposite effect on both I_c and S, where evanescent states have a tendency to sinusoidal behavior and are more relevant in the short-junction regime since they possess a decay length.

The temperature dependence of S is illustrated in Fig. 5(c); in both the short- and long-junction regimes S exhibits a concavity change. The maximum S value that can be attained at zero temperature depends on doping, edge type, and junction length. For long junctions, S decays more rapidly with temperature, which can be explained by the fact that the normal modes' transmission probability diminishes as junction length

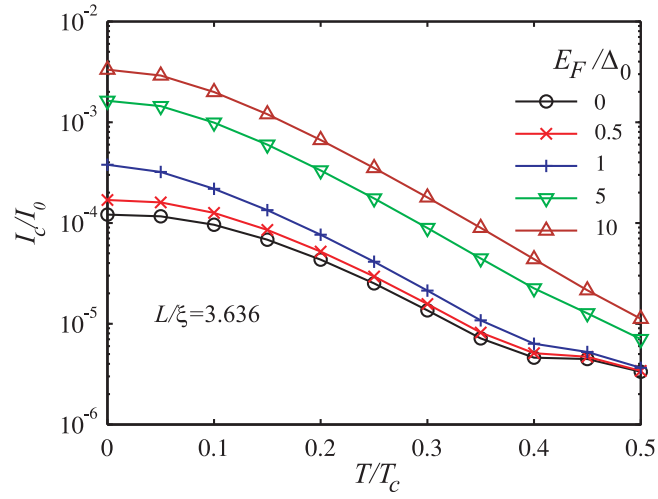

FIG. 6. Temperature dependence of (a) the critical current and (b) skewness for an SGS Josephson junction with a zigzag edge. The exponential decay law is evaluated for the long-junction case, $L/\xi = 3.636$.

increases and, as has been pointed out by other authors [14], the population of continuum states decreases. The temperature dependences of I_c and S at finite doping are in agreement with measurements in a recent work [14] on the ballistic Josephson junction with *h*BN encapsulated graphene.

Figure 6 shows, in a semilogarithmic plot, the temperature dependence of the critical current in the long-junction regime ($L/\xi \approx 3.636$); the linearity obtained for certain doping values means an exponential decay law, which was measured recently [15]. This result is in agreement with those obtained for conventional SNS junctions at low temperatures. For doping values near the Dirac point, the exponential decay is not maintained. Figure 5(c) shows that in the long-junction regime skewness decays more rapidly.

IV. CONCLUSIONS

In this work we have given a general characterization of the current phase relationship for short- and long-junction regimes. We showed that critical current and skewness exhibit critical points as a function of graphene doping. The location of these critical points was explained and related to resonance conditions due to Klein tunneling and nanoribbon quasibound states, and we showed that critical current and skewness curves are correlated. When the continuum contribution is taken into account, the skewness values are always positive in both short- and long-junction regimes.

We have calculated the temperature dependence of the critical current and skewness. The critical current exhibits a behavior with concavity change, except at very low doping values in the short-junction regime, where the curve shows a temperature behavior similar to that observed in conventional SIS and ScS junctions. For long junctions we showed that the critical current exhibits an exponential decay law.

We obtained the relationship between skewness and the critical current by fixing doping or temperature. When doping is constant, the behavior is nonlinear, and the slope of the

curve depends on junction length. We showed that when temperature is constant, skewness oscillates as a function of critical current, and its oscillations are more pronounced when the temperature is decreased.

The effect of nonideal interfaces was included; we found that when interfaces have transparency below unity, the zigzag case displays critical current and skewness curves which have a similar behavior and are out of phase with respect to those obtained for the armchair case. The reason is the interplay between Klein resonances and standard quantum tunneling.

Our approach based on the perturbed Green's function of the Josephson junction takes into account the different contributions of quasibound states, evanescent states, and the continuum to the electric transport properties. The formalism allows us to determine the full doping and temperature dependence of the skewness and critical current; the results were obtained without restriction of junction length. The above makes a comparison with recent experimental results [14,15,21] possible. Contrary to other theoretical approaches, we can obtain skewness behavior for low doping values [14]. The exponential temperature decay law of the critical current was measured recently [15] and is in agreement with our results. The relation between the skewness and critical current obtained in this work can help to explain a recent experimental result [21]. The skewness is a feature of graphene Josephson junctions that has been little studied; motivated by recent experimental works [14,21], we expect that our research may contribute to the understanding of the current phase relation of graphene Josephson junctions. Overall, the SGS Josephson junction has different characteristics with the advantage of tunability of the graphene monolayer; the ballistic transport was possible with *h*BN encapsulated graphene. Therefore, we expect that new experiments on Josephson junctions with well-defined edges will arise in the low-doping regime to test some results of our work.

ACKNOWLEDGMENT

We acknowledge funding from COLCIENCIAS, Project No. 110165843163.

APPENDIX: JOSEPHSON CURRENT FOR AN SGS JUNCTION

The current between two regions, L and R, is given in general by Eq. (2); in the SGS system self-energies model coupling between superconducting and normal graphene regions, which have a well-defined edge. P_L and P_R are hopping parameters between superconductor and graphene regions (see Fig 1). The description involves a Nambu representation together with a sublattice structure, which leads to a 4×4 matrix structure for Green's functions and self-energies. For the zigzag case, the self-energies can be written as

$$\tilde{\Sigma}^{\dagger}_{RL}=\tilde{\Sigma}_{LR}=p_{L(R)}\begin{pmatrix}\sigma_1^T & 0\\ 0 & -\sigma_1^T\end{pmatrix},\quad \sigma_1=\begin{pmatrix}0 & 1\\ 0 & 0\end{pmatrix}, \tag{A1}$$

with $p_{L(R)}=\hbar v_F P_{L(R)}$; instead, for the armchair case we can factorize the self-energy in Eq. (2) since

$$\tilde{\Sigma}_{RL}=\tilde{\Sigma}_{LR}=p_{L(R)}\begin{pmatrix}\hat{\sigma}_x & 0\\ 0 & -\hat{\sigma}_x\end{pmatrix},\quad \hat{\sigma}_x=\begin{pmatrix}0 & 1\\ 1 & 0\end{pmatrix}. \tag{A2}$$

The indices L and R stand for the two graphene superconductor interfaces in the SGS system. In equilibrium, we can use

$$\tilde{G}^{+-}_{RL(LR)}(E,k_y)=\left[\tilde{G}^{a}_{RL(LR)}(E,k_y)-\tilde{G}^{r}_{RL(LR)}(E,k_y)\right]f(E), \tag{A3}$$

where $f(E)$ is the Dirac-Fermi distribution for quasiparticles. With the above property and Eqs. (A1) and (A2), the current given by Eq. (2) can be written for the armchair and zigzag cases as

$$\begin{aligned}I_{\rm arm}=\frac{2ep_L}{h}\int_0^{\infty}\int_{-k_c}^{-k_c}&{\rm Re}\big\{G^r_{LReeBA}(E,k_y)+G^r_{LReeAB}(E,k_y)+G^r_{LRhhBA}(E,k_y)+G^r_{LRhhAB}(E,k_y)\\&-G^r_{RLeeAB}(E,k_y)-G^r_{RLeeBA}(E,k_y)-G^r_{RLhhAB}(E,k_y)-G^r_{RLhhBA}(E,k_y)\big\}[2f(E)-1]dk_ydE\end{aligned} \tag{A4}$$

and

$$I_{zig}=\frac{2ep_L}{h}\int_0^{\infty}\int_{-k_c}^{-k_c}{\rm Re}\big\{G^r_{LReeBA}(E,k_y)+G^r_{LRhhBA}(E,k_y)-G^r_{RLeeAB}(E,k_y)-G^r_{RLhhAB}(E,k_y)\big\}[2f(E)-1]dk_ydE. \tag{A5}$$

Re indicates the real part. The Green's functions $\tilde{G}^r_{RL(LR)}$ are 4×4 matrices, where *ee* (*hh*) denotes electron (hole) submatrices in Nambu space and A (B) designates the sublattice graphene space. The nonlocal perturbed Green's functions $\tilde{G}^r_{RL(LR)}$ can be obtained through the algebraic Dyson equation

$$\tilde{G}_{RL}=\tilde{G}_{RR}\tilde{\Sigma}_{RL}\tilde{g}_{LL}, \tag{A6}$$

$$\tilde{G}_{LR}=\tilde{g}_{LL}\tilde{\Sigma}_{LR}\tilde{G}_{RR}, \tag{A7}$$

where $\tilde{G}_{RR}$ is the perturbed Green's function of the SGS system and $\tilde{g}_{LL}$ is the nonperturbed Green's function of the left superconductor. To obtain $\tilde{G}_{RR}$ it is necessary to solve two successive Dyson equations similar to Eqs. (A6) and (A7) at $x=0$ and $x=-L$ (see Fig. 1), where the input functions are the nonperturbed Green's functions for left and right superconductors and the graphene nanoribbon, which were obtained previously [26].

The Dyson equation is solved numerically for the armchair case due to a more complex matrix structure. The zigzag case has more zero matrix components, which allows us to obtain an analytical expression for the nonlocal Green's functions. As an

example, we write the expression for the perturbed nonlocal Green's function $\tilde{G}^r_{LR}$ in the limit of a heavily doped superconductor; we obtain

$$\tilde{G}^r_{LR}(E,k_y)=\left(\frac{-i}{\hbar v}\right)^2 p_L \begin{pmatrix} -1 & 0 & 0 & 0 \\ \frac{1}{\Omega}E & 0 & -\frac{\Delta}{\Omega}e^{i\varphi} & 0 \\ 0 & 0 & -1 & 0 \\ \frac{\Delta}{\Omega}e^{-i\varphi} & 0 & -\frac{1}{\Omega}E & 0 \end{pmatrix} \left[I - \frac{P_L^2}{D_2} \begin{pmatrix} J_e & 0 & -K & 0 \\ 1 & 0 & 0 & 0 \\ -K & 0 & J_h & 0 \\ 0 & 0 & -1 & 0 \end{pmatrix} \right. \times \left. \begin{pmatrix} \frac{\Delta}{\Omega}S_h e^{-i\varphi} - T_h\frac{1}{\Omega}E & 0 & -\frac{1}{\Omega}ES_h + \frac{\Delta}{\Omega}T_h e^{i\varphi} & 0 \\ 0 & 0 & 0 & 0 \\ \frac{\Delta}{\Omega}T_e e^{-i\varphi} - S_e\frac{1}{\Omega}E & 0 & -\frac{1}{\Omega}ET_e + \frac{\Delta}{\Omega}S_e e^{i\varphi} & 0 \\ 0 & 0 & 0 & 0 \end{pmatrix} \right] \begin{pmatrix} J_e & -1 & -K & 0 \\ 0 & 0 & 0 & 0 \\ -K & 0 & J_h & 1 \\ 0 & 0 & 0 & 0 \end{pmatrix}, \tag{A8}$$

where we have defined the auxiliary quantities

$$k_{e(h)} = s_\pm\left[\tilde{E}_\pm^2 - k_y^2\right]^{1/2}, \quad e^{i\alpha_{e(h)}} = \frac{k_{e(h)} + ik_y}{\tilde{E}_\pm}, \quad \tilde{E}_\pm = (E_F \pm E)/\hbar v_F,\ s_\pm = \mathrm{sgn}(E_F \pm E), \tag{A9}$$

$$c_{e(h)} = \frac{e^{\mp i\alpha_{e(h)}}(1 - e^{\pm 2ik_{e(h)}L})}{1 + e^{\mp 2i\alpha_{e(h)}}e^{\pm 2ik_{e(h)}L}}, \quad d_{e(h)} = \frac{e^{\pm ik_{e(h)}L}(1 + e^{\mp 2i\alpha_{e(h)}})}{(1 + e^{\mp 2i\alpha_{e(h)}}e^{\pm 2ik_{e(h)}L})}, \tag{A10}$$

$$J_{e(h)} = c_{e(h)} - \frac{P_R^2}{D_1}d_{e(h)}^2\left(P_R^2 c_{h(e)} + \frac{E}{\Omega}\right), \quad K = \frac{P_R^2}{D_1}\frac{\Delta}{\Omega}d_e d_h, \tag{A11}$$

$$S_{e(h)} = \frac{\Delta}{\Omega}e^{\mp i\varphi}P_L^2 J_{e(h)} + P_L^2 K\frac{E}{\Omega}, \quad T_{e(h)} = 1 + \frac{E}{\Omega}P_L^2 J_{e(h)} + P_L^2 K\frac{\Delta}{\Omega}e^{\pm i\varphi}, \tag{A12}$$

$$D_1 = -1 - 2P_R^2\frac{E}{\Omega}\frac{c_e + c_h}{2} - P_R^4 c_e c_h, \tag{A13}$$

$$F = 2K\frac{\Delta}{\Omega}, \quad G = -\frac{E}{\Omega}(J_e + J_h)P_L^2 + P_L^4(K^2 - J_e J_h), \tag{A14}$$

$$D_2(\varphi) = -1 - 2P_L^2 F\cos\varphi + G.a \tag{A15}$$

The current through the junction is obtained by inserting Eq. (A8) and other similar expressions for $\tilde{G}^r_{RL}$ into Eq. (A5), which leads to Eq. (4). The result shows that φ dependence is nonsinusoidal because the behavior is affected by a factor that depends on the phase difference. In the tunnel limit the factors $D_1, D_2(\varphi)$ are equal to the unity; therefore, a sinusoidal behavior is recovered.

[1] H. B. Heersche, P. Jarillo-Herrero, J. B. Oostinga, L. M. K. Vandersypen, and A. F. Morpurgo, Nature (London) **446**, 56 (2007).

[2] X. Du, I. Skachko, and E. Y. Andrei, Phys. Rev. B **77**, 184507 (2008).

[3] V. E. Calado, S. Goswami, G. Nanda, M. Diez, A. R. Akhmerov, K. Watanabe, T. Taniguchi, T. M. Klapwijk, and L. M. K. Vandersypen, Nat. Nanotechnol. **10**, 761 (2015).

[4] L. Bretheau, J. I-Jan Wang, R. Pisoni, K. Watanabe, T. Taniguchi, and P. Jarillo-Herrero, Nat. Phys. **13**, 756 (2017).

[5] M. B. Shalom, M. J. Zhu, V. I. Fal'ko, A. Mishchenko, A. V. Kretinin, K. S. Novoselov, C. R. Woods, K. Watanabe, T. Taniguchi, A. K. Geim, and J. R. Prance, Nat. Phys. **12**, 318 (2016).

[6] I. O. Kulik, Sov. Phys. JETP **30**, 944 (1970).

[7] A. A. Golubov, M. Y. Kupriyanov, and E. Il'ichev, Rev. Mod. Phys. **76**, 411 (2004).

[8] G.-H. Lee and H.-J. Lee, Rep. Prog. Phys. **81**, 056502 (2018).

[9] A. F. Young and P. Kim, Nat. Phys. **5**, 222 (2009).

[10] J. M. Pereira, Jr., P. Vasilopoulos, and F. M. Peeters, Appl. Phys. Lett. **90**, 132122 (2007).

[11] M. I. Katsnelson, K. S. Novoselov, and A. K. Geim, Nat. Phys. **2**, 620 (2006).

[12] J. M. Pereira, Jr., V. Mlinar, F. M. Peeters, and P. Vasilopoulos, Phys. Rev. B **74**, 045424 (2006).

[13] I. Rodríguez-Vargas, J. Madrigal-Melchor, and O. Oubram, J. Appl. Phys. **112**, 073711 (2012).

[14] G. Nanda, J. L. Aguilera-Servin, P. Rakyta, A. Kormányos, R. Kleiner, D. Koelle, K. Watanabe, T. Taniguchi, L. M. K. Vandersypen, and S. Goswami, Nano Lett. **17**, 3396 (2017).

[15] I. V. Borzenets, F. Amet, C. T. Ke, A. W. Draelos, M. T. Wei, A. Seredinski, K. Watanabe, T. Taniguchi, Y. Bomze, M. Yamamoto, S. Tarucha, and G. Finkelstein, Phys. Rev. Lett. **117**, 237002 (2016).

[16] T. Li, J. Gallop, L. Hao, and E. Romans, Supercond. Sci. Technol. **31**, 045004 (2018).

[17] F. E. Schmidt, M. D. Jenkins, K. Watanabe, T. Taniguchi, and G. A. Steele, Nat. Commun. **9**, 4069 (2018).

[18] E. Sarvestani and S. A. Jafari, Phys. Rev. B **85**, 024513 (2012).

[19] I. Hagymási, A. Kormányos, and J. Cserti, Phys. Rev. B **82**, 134516 (2010).

[20] A. M. Black-Schaffer and J. Linder, Phys. Rev. B **82**, 184522 (2010).

[21] C. D. English, D. R. Hamilton, C. Chialvo, I. C. Moraru, N. Mason, and D. J. Van Harlingen, Phys. Rev. B **94**, 115435 (2016).

[22] P. Ruffieux, S. Wang, B. Yang, C. Sánchez-Sánchez, J. Liu, T. Dienel, L. Talirz, P. Shinde, C. A. Pignedoli, D. Passerone, T. Dumslaff, X. Feng, K. Müllen, and R. Fasel, Nature (London) **531**, 489 (2016).

[23] J. Cai, P. Ruffieux, R. Jaafar, M. Bieri, T. Braun, S. Blankenburg, M. Muoth, A. P. Seitsonen, M. Saleh, X. Feng, K. Müllen, and R. Fasel, Nature (London) **466**, 470 (2010).

[24] D. Lungerich, O. Papaianina, M. Feofanov, J. Liu, M. Devarajulu, S. I. Troyanov, S. Maier, and K. Amsharov, Nat. Commun **9**, 4756 (2018).

[25] A. Zakharov, N. A. Vinogradov, J. Aprojanz, T. T. N. Nguyen, C. Tegenkamp, C. Struzzi, T. Iakimov, R. Yakimova, and V. Jokubavicius, ACS Appl. Nano Mater. **2**, 156 (2019).

[26] W. J. Herrera, P. Burset, and A. L. Yeyati, J. Phys.-Condens. Mat. **22**, 275304 (2010).

[27] M. Titov and C. W. J. Beenakker, Phys. Rev. B **74**, 041401(R) (2006).

[28] A. H. Castro Neto, F. Guinea, N. M. R. Peres, K. S. Novoselov, and A. K. Geim, Rev. Mod. Phys. **81**, 109 (2009).

[29] V. S. Shumeiko, E. N. Bratus, and G. Wendin, Low Temp. Phys. **23**, 181 (1997).

[30] K. K. Likharev, Rev. Mod. Phys. **51**, 101 (1979).